Available online at www.sciencedirect.com

ScienceDirect

IFAC Papers Online CONFERENCE PAPER ARCHIVE

IFAC PapersOnLine 51-13 (2018) 186–191

Pose Estimation using Dual Quaternions and Moving Horizon Estimation ⋆

Aksel Sveier * **Olav Egeland** *

* *Department of Mechanical and Industrial Engineering, Norwegian University of Science and Technology (NTNU), 7491 Trondheim, Norway (e-mail: aksel.sveier, olav.egeland@ntnu.no)*

Abstract: This paper presents a moving horizon estimator (MHE) for estimating pose (attitude and position) of a dynamic system where pose measurements are available in the form of unit dual quaternions. A unit dual quaternion is an 8 parameter nonsingular representation of pose and has previously been used for pose estimation with Kalman filters (KF). We formulate a cost function in terms of the quaternion product and propose a MHE that includes the N latest measurements in the estimation. In addition, we suggest a measurement relation based on the Cayley transform of the noise, where the noise has a Gaussian distribution about the *x-y-z* and *roll-pitch-yaw* parameters of the pose. The MHE is compared against the dual quaternion multiplicative extended KF (DQ-MEKF) and the twistor-based unscented KF (T-UKF) through 100 Monte Carlo simulations, where the simulated data is generated according to the defined system dynamics. It is found that the MHE gives more accurate pose estimation results.

Keywords: Dual Quaternions, Pose Estimation, Moving Horizon Estimation, Kalman Filtering

1. INTRODUCTION

Relative pose estimation of systems with six degrees of freedom has broad application in relative navigation, 3D mapping and robotics. Traditionally, pose estimation has been divided into two problems of estimating position and attitude. The attitude is represented by a 3×3 rotation matrix $\mathbf{R} \in \mathrm{SO}(3)$ and the position by a 3 dimensional Euclidean vector $\mathbf{t} \in \mathbb{R}^3$. In state estimation, the state can only contain column vectors, therefore the attitude is usually parameterized using Euler angles, Rodrigues parameters (RP), Modified RP (MRP) or a unit quaternion (Chaturvedi et al., 2011). By considering unit *dual* quaternions, it is no longer necessary to divide the pose estimation problem into two separate estimation problems. Unit dual quaternions provide a global nonsingular representation of pose with 8 parameters and are well suited for simultaneous attitude and position estimation. Kalman filtering (KF) techniques for pose estimation using dual quaternions has been developed in the recent years with good results (Goddard, 1997; Bayro-Corrochano and Zhang, 2000; Zu et al., 2014; Filipe et al., 2015; Deng et al., 2016). These estimators consider only the most recent measurement in the update and assume that all previous measurements are optimally accounted for in the current state, which for extended KFs (EKF) and Unscented KFs (UKF) are approximations, as these filters are not optimal due to linearization.

Moving Horizon Estimation (MHE) is a state estimation method that uses the N most recent measurements, containing noise, and optimizes the state estimate about the defined system dynamics such that the noise is minimized. MHE has been used in combination with model predictive control for process control problems (Kristoffersen and Holden, 2018) and has also been applied to the problem of pose estimation (Geebelen et al., 2013; Polóni et al., 2015). In Vandersteen et al. (2013) the attitude of a spacecraft is estimated with a MHE, where the attitude is represented with a unit quaternion. The unit constraint of the quaternion is enforced by including it as an explicit constraint of the optimization problem.

In this paper, we extend the method in Vandersteen et al. (2013) to pose estimation using unit dual quaternions. We formulate a cost function in terms of the quaternion product so that the unit constraint of the unit dual quaternion will be satisfied. In addition, we use the Cayley transform (Selig, 2010) for dual vectors to model the effect of noise in the unit dual quaternion measurements. This ensures that the measurement dual quaternion has unit length and we avoid projection and normalization. Furthermore, we show that our proposed measurement model generate pose results that are Gaussian distributed about the *roll-pitch-yaw* and *x-y-z* parameters. Lastly, we compare the dual quaternion multiplicative EKF (DQ-MEKF) (Filipe et al., 2015) and the twistor-based UKF (T-UKF) (Deng et al., 2016) with our proposed MHE using simulated data and find that the MHE is the most accurate. This can be explained by the fact that the MHE includes several previous measurements in the estimation and does not assume that all previous information is fully accounted for in the current state, which is a key assumption in Kalman filtering.

The paper is organized as follows: Sect. 2.1 and Sect. 2.2 presents notation and preliminary results of quaternions and dual quaternions. Sect. 2.3 present the continuous quaternion kinematics, which describes the dynamics of the considered system and Sect. 2.4 show how this system can be discretized using the Cayley transform (Selig, 2010). Sect. 3 introduce the MHE problem and the formu-

⋆ The research presented in this paper has received funding from the Norwegian Research Council, SFI Offshore Mechatronics, project number 237896.

10.1016/j.ifacol.2018.07.275

lation of the cost function in terms of the system dynamics. Sect. 4 show the simulations and results, while Sect. 5 concludes the paper.

2. PRELIMINARIES

2.1 Quaternions

A quaternion can be represented as a sum $\mathbf{q} = \eta + \boldsymbol{\sigma}$ of a scalar $\eta \in \mathbb{R}$ and a vector $\boldsymbol{\sigma} \in \mathbb{R}^3$. The quaternion can also be represented as a column vector $[\mathbf{q}] = \begin{bmatrix} \eta & \boldsymbol{\sigma}^\top \end{bmatrix}^\top$. Conjugation is given by $\mathbf{q}^* = \eta - \boldsymbol{\sigma}$, and multiplication with a scalar λ gives $\lambda\mathbf{q} = \lambda\eta + \lambda\boldsymbol{\sigma}$. Addition of two quaternions $\mathbf{q}_1 = \eta_1 + \boldsymbol{\sigma}_1$ and $\mathbf{q}_2 = \eta_2 + \boldsymbol{\sigma}_2$ is done component-wise and gives $\mathbf{q}_1 + \mathbf{q}_2 = (\eta_1 + \eta_2) + (\boldsymbol{\sigma}_1 + \boldsymbol{\sigma}_2)$. The subtraction of two quaternions is analogous to the addition. The quaternion product is denoted with $\otimes$ and is defined by $\mathbf{q}_1 \otimes \mathbf{q}_2 = (\eta_1\eta_2 - \boldsymbol{\sigma}_1 \cdot \boldsymbol{\sigma}_2) + (\eta_1\boldsymbol{\sigma}_2 + \eta_2\boldsymbol{\sigma}_1 + \boldsymbol{\sigma}_1 \times \boldsymbol{\sigma}_2)$. A vector $\mathbf{v}$ can be treated as a quaternion with zero scalar part, and the quaternion product between a vector and a quaternion is then $\mathbf{q} \otimes \mathbf{v} = -\boldsymbol{\sigma} \cdot \mathbf{v} + (\eta\mathbf{v} + \boldsymbol{\sigma} \times \mathbf{v})$. The magnitude of a quaternion is $\|\mathbf{q}\|^2 = \mathbf{q} \otimes \mathbf{q}^* = [\mathbf{q}]^\top[\mathbf{q}] = \eta^2 + \boldsymbol{\sigma} \cdot \boldsymbol{\sigma}$ and the inverse is given by $\mathbf{q}^{-1} = \mathbf{q}^* / \|\mathbf{q}\|^2$.

A unit quaternion $\mathbf{q}$ has unit magnitude $\|\mathbf{q}\|^2 = 1$ and is used to represent attitude for objects and moving vehicles (Lefferts et al., 1982). Given a rotation θ about an axis given by the unit vector $\mathbf{k}$ through the origin, the unit quaternion describing the rotation is given by $\mathbf{q} = \cos\frac{\theta}{2} + \sin\frac{\theta}{2}\mathbf{k}$. This unit quaternion is also given by the exponential function

$$\mathbf{q} = \exp\left(\frac{\theta\mathbf{k}}{2}\right) = 1 + \left(\frac{\theta\mathbf{k}}{2}\right) + \frac{1}{2}\left(\frac{\theta\mathbf{k}}{2}\right)^2 + \dots, \quad (1)$$

where $(\cdot)^i$ denotes the quaternion product of order i. The corresponding rotation matrix $\mathbf{R} \in \mathrm{SO}(3)$ is given by $\mathbf{R}(\mathbf{q}) = \mathbf{I} + 2\eta\boldsymbol{\sigma}^\times + 2\boldsymbol{\sigma}^\times\boldsymbol{\sigma}^\times$, where $(\cdot)^\times$ denotes the skew symmetric matrix and $\mathbf{I}$ is the identity matrix. For $-\pi \leq \theta \leq \pi$ the scalar part of a unit quaternion can be recovered through the relation $\eta = \sqrt{1 - \|\boldsymbol{\sigma}\|^2}$.

2.2 Dual Quaternions

A dual quaternion is given by $\tilde{\mathbf{q}} = \mathbf{q} + \varepsilon\mathbf{q}'$ where the real part $\mathbf{q}$ and the dual part $\mathbf{q}'$ are quaternions (Filipe et al., 2015). Here, ε is the dual unit and is defined by $\varepsilon \neq 0$ and $\varepsilon^2 = 0$. The dual quaternion can also be represented by the column vector $[\tilde{\mathbf{q}}] = [[\mathbf{q}]^\top \ [\mathbf{q}']^\top]^\top$. Conjugation is given by $\tilde{\mathbf{q}}^* = \mathbf{q}^* + \varepsilon\mathbf{q}'^*$, and multiplication with a scalar λ gives $\lambda\tilde{\mathbf{q}} = \lambda\mathbf{q} + \varepsilon\lambda\mathbf{q}'$. Addition of two dual quaternions $\tilde{\mathbf{q}}_1 = \mathbf{q}_1 + \varepsilon\mathbf{q}'_1$ and $\tilde{\mathbf{q}}_2 = \mathbf{q}_2 + \varepsilon\mathbf{q}'_2$ gives $\tilde{\mathbf{q}}_1 + \tilde{\mathbf{q}}_2 = (\mathbf{q}_1 + \mathbf{q}_2) + \varepsilon(\mathbf{q}'_1 + \mathbf{q}'_2)$. The quaternion product of two dual quaternions is given by $\tilde{\mathbf{q}}_1 \otimes \tilde{\mathbf{q}}_2 = \mathbf{q}_1 \otimes \mathbf{q}_2 + \varepsilon(\mathbf{q}_1 \otimes \mathbf{q}'_2 + \mathbf{q}'_1 \otimes \mathbf{q}_2)$. A dual vector $\tilde{\mathbf{v}} = \mathbf{v} + \varepsilon\mathbf{v}'$, where $\mathbf{v}$ and $\mathbf{v}'$ are vectors, can be treated as a dual quaternion with zeros scalar parts, and the quaternion product is $\tilde{\mathbf{q}} \otimes \tilde{\mathbf{v}} = \mathbf{q} \otimes \mathbf{v} + \varepsilon(\mathbf{q} \otimes \mathbf{v}' + \mathbf{q}' \otimes \mathbf{v})$. The dual magnitude of a dual quaternion is $\|\tilde{\mathbf{q}}\|^2 = \tilde{\mathbf{q}} \otimes \tilde{\mathbf{q}}^* = \mathbf{q} \otimes \mathbf{q}^* + \varepsilon(\mathbf{q} \otimes \mathbf{q}'^* + \mathbf{q}' \otimes \mathbf{q}^*)$ and the inverse is $\tilde{\mathbf{q}}^{-1} = \tilde{\mathbf{q}}^* / \|\tilde{\mathbf{q}}\|^2$.

The unit dual quaternion is subject to the constraint $\|\tilde{\mathbf{q}}\| = 1$ and is used to describe the pose or displacement of a rigid body (McCarthy and Soh, 2010). A displacement can be described as a screw motion, which is a rotation by an angle θ about a line $\tilde{\mathbf{k}} = \mathbf{k} + \varepsilon\mathbf{k}'$ and a translation d along the same line. The dual angle is written as $\tilde{\theta} = \theta + \varepsilon d$. The unit dual quaternion describing the motion is then $\tilde{\mathbf{q}} = \cos\frac{\tilde{\theta}}{2} + \sin\frac{\tilde{\theta}}{2}\tilde{\mathbf{k}}$. The unit dual quaternion is also given by the exponential function

$$\exp\left(\frac{\tilde{\theta}\tilde{\mathbf{k}}}{2}\right) = 1 + \left(\frac{\tilde{\theta}\tilde{\mathbf{k}}}{2}\right) + \frac{1}{2}\left(\frac{\tilde{\theta}\tilde{\mathbf{k}}}{2}\right)^2 + \dots, \quad (2)$$

where $(\cdot)^i$ denotes the quaternion product of order i. The corresponding homogeneous transformation matrix $\mathbf{T} \in \mathrm{SE}(3)$ is given by

$$\mathbf{T}(\tilde{\mathbf{q}}) = \begin{bmatrix} \mathbf{R}(\mathbf{q}) & 2\mathbf{q}' \otimes \mathbf{q}^* \\ \mathbf{0}^\top & 1 \end{bmatrix}. \quad (3)$$

2.3 Continuous Quaternion Kinematics

Consider the body frame B and a reference inertial frame I. The attitude of B with respect to the reference frame I is described with the unit quaternion $\mathbf{q}_{B/I} = \mathbf{q}$. The angular velocity of the body frame with respect to the reference frame described in the body frame is denoted with the vector $\boldsymbol{\omega}^B_{B/I} = \boldsymbol{\omega}^B$. The kinematic differential equation describing the system is

$$\dot{\mathbf{q}} = \frac{1}{2}\mathbf{q} \otimes \boldsymbol{\omega}^B. \quad (4)$$

Consider the displacement of B described by the unit dual quaternion $\tilde{\mathbf{q}}_{B/I} = \tilde{\mathbf{q}}$, then the twist of the displacement is a screw given by the dual vector $\tilde{\boldsymbol{\omega}}^B = \boldsymbol{\omega}^B + \varepsilon\mathbf{v}^B$ given in the body frame B. Here, $\mathbf{v}^B$ is the linear velocity of the body frame. The kinematic differential equation describing the displacement of the system is given by

$$\dot{\tilde{\mathbf{q}}} = \frac{1}{2}\tilde{\mathbf{q}} \otimes \tilde{\boldsymbol{\omega}}^B. \quad (5)$$

2.4 Discrete Quaternion Kinematics

In the discretization of the kinematic differential equation (4), it is possible to use a formulation that that will ensure that the algebraic constraint of the unit quaternion will be satisfied. Such an integrator could be the exponential function (1), which gives the discrete-time system

$$\mathbf{q}_{k+1} = \mathbf{q}_k \otimes \exp\left(\frac{h}{2}\boldsymbol{\omega}^B_k\right), \quad (6)$$

where h is the time step and the subscript k denotes the time instance t_k. Then $\mathbf{q}_{k+1}$ will be the result of a rotation with constant angular velocity $\boldsymbol{\omega}^B_k$ over the time interval h from $\mathbf{q}_k$.

We will use another geometric integrator based on the Cayley transform (Selig, 2010), which has a simple solution with exact results and an exact inverse. The Cayley transform of a vector $\mathbf{u}$ is defined as

$$\mathrm{cay}\,(\mathbf{u}) \triangleq (1 + \mathbf{u}) \otimes (1 - \mathbf{u})^{-1}. \quad (7)$$

Using the definition of the inverse quaternion gives

$$\mathrm{cay}\,(\mathbf{u}) = \frac{(1 + \mathbf{u}) \otimes (1 - \mathbf{u}^*)}{(1 - \mathbf{u}) \otimes (1 - \mathbf{u}^*)} = \frac{1 - \mathbf{u}^2}{1 + \mathbf{u}^2} + \frac{2\mathbf{u}}{1 + \mathbf{u}^2}.$$

From this it is straightforward to show that $\|\mathrm{cay}\,(\mathbf{u})\| = 1$, and it is concluded that $\mathrm{cay}\,(\mathbf{u})$ is a unit quaternion. From standard geometric identities it follows that

$$\mathrm{cay}\left(\mathbf{k}\tan\frac{\theta}{4}\right) = \cos\frac{\theta}{2} + \mathbf{k}\sin\frac{\theta}{2} = \exp\left(\frac{\theta\mathbf{k}}{2}\right). \quad (8)$$

The approximation $\tan\theta \approx \theta$ can be used for small angles and the Cayley transform is therefore an approximation of the exponential function for small angles

$$\text{cay}\left(\frac{1}{2}\frac{\theta\mathbf{k}}{2}\right) \approx \exp\left(\frac{\theta\mathbf{k}}{2}\right). \tag{9}$$

The Cayley transform of a twist $\tilde{\mathbf{u}} = \mathbf{u} + \varepsilon\mathbf{u}'$ is defined similarly to (7) as

$$\text{cay}\left(\tilde{\mathbf{u}}\right) \triangleq (1+\tilde{\mathbf{u}}) \otimes (1-\tilde{\mathbf{u}})^{-1}. \tag{10}$$

Then

$$\text{cay}\left(\tilde{\mathbf{u}}\right) = \frac{(1+\tilde{\mathbf{u}}) \otimes (1-\tilde{\mathbf{u}}^*)}{(1-\tilde{\mathbf{u}}) \otimes (1-\tilde{\mathbf{u}}^*)} = \frac{1-\tilde{\mathbf{u}}^2}{1+\tilde{\mathbf{u}}^2} + \frac{2\tilde{\mathbf{u}}}{1+\tilde{\mathbf{u}}^2},$$

from which it is straightforward to show that $\|\text{cay}\left(\tilde{\mathbf{u}}\right)\| = 1$. This means that $\text{cay}\left(\tilde{\mathbf{u}}\right)$ is a unit dual quaternion. Because the standard trigonometric identities also applies for trigonometric functions of dual angles, it follows that

$$\text{cay}\left(\tilde{\mathbf{k}}\tan\frac{\tilde{\theta}}{4}\right) = \cos\frac{\tilde{\theta}}{2} + \tilde{\mathbf{k}}\sin\frac{\tilde{\theta}}{2} = \exp\left(\frac{\tilde{\theta}\tilde{\mathbf{k}}}{2}\right). \tag{11}$$

Because $\tan\tilde{\theta} \approx \tilde{\theta}$ for small dual angles $\tilde{\theta}$, it follows that the Cayley transform is an approximation of the exponential function

$$\text{cay}\left(\frac{1}{2}\frac{\tilde{\theta}\tilde{\mathbf{k}}}{2}\right) \approx \exp\left(\frac{\tilde{\theta}\tilde{\mathbf{k}}}{2}\right), \tag{12}$$

where the rotation is about the same axis $\tilde{\mathbf{k}}$, while the angle of rotation is a first-order approximation. The discrete kinematics of a system describing displacement can, therefore, be approximated by

$$\tilde{\mathbf{q}}_{k+1} = \tilde{\mathbf{q}}_k \otimes \text{cay}\left(\frac{h}{4}\tilde{\boldsymbol{\omega}}_k^B\right). \tag{13}$$

Then $\tilde{\mathbf{q}}_{k+1}$ will be a unit dual quaternion whenever $\tilde{\mathbf{q}}_k$ is a unit dual quaternion.

It is noted that the inverse Cayley transform of a unit dual quaternion $\tilde{\mathbf{q}}$ is a dual vector representing a twist, which is given by

$$\text{cay}^{-1}\left(\tilde{\mathbf{q}}\right) = (\tilde{\mathbf{q}}-1) \otimes (\tilde{\mathbf{q}}+1)^{-1}. \tag{14}$$

3. ESTIMATION PROBLEM

The MHE problem is formulated with a cost function that is solved with nonlinear programming solvers. The formulation of the cost function can be ad hoc and not necessarily justified. It is therefore up to the designer to formulate a reasonable cost function, and this can be done even for highly nonlinear and constrained problems (Rawlings and Mayne, 2015). The MHE reduces to the linear KF when the system is linear, unconstrained and the noise is Gaussian. Moreover, the MHE produce optimal results even when the system is nonlinear and constrained, contrary to recursive filters such as the EKF and the UKF, which approximates the estimates through linearization.

Consider the discrete nonlinear system

$$\mathbf{x}_{k+1} = f(\mathbf{x}_k) + \mathbf{w}_k \tag{15}$$
$$\mathbf{y}_k = h(\mathbf{x}_k) + \mathbf{v}_k, \tag{16}$$

where $\mathbf{x}_k$ is a vector describing the state, $\mathbf{y}_k$ is a measurement of $\mathbf{x}_k$ and $\mathbf{w}_k$ and $\mathbf{v}_k$ are Gaussian noise. Then the MHE problem can be defined as follows:

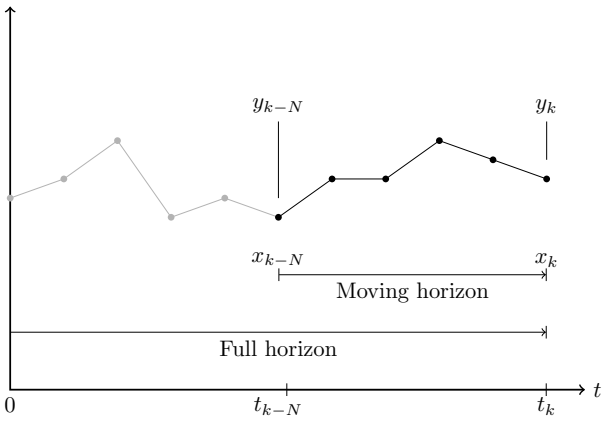

Fig. 1. Moving horizon estimation problem.

$$\begin{aligned}\underset{\substack{\mathbf{x}_{k-N},\ldots,\mathbf{x}_k\\ \mathbf{w}_{k-N},\ldots,\mathbf{w}_{k-1}\\ \mathbf{v}_{k-N},\ldots,\mathbf{v}_k}}{\text{minimize}} \; & \frac{1}{2}\sum_{i=k-N}^{k-1}\mathbf{w}_i^\top\mathbf{Q}^{-1}\mathbf{w}_i \\ & + \frac{1}{2}\sum_{i=k-N}^{k}\mathbf{v}_i^\top\mathbf{R}^{-1}\mathbf{v}_i \\ & + \frac{1}{2}(x_{k-N}^- - x_{k-N})^\top\mathbf{P}^{-1}(x_{k-N}^- - x_{k-N})\end{aligned} \tag{17}$$

subject to

$$\mathbf{x}_{i+1} = f(\mathbf{x}_i) + \mathbf{w}_i \text{ for } i = k-N,\ldots,N-1 \tag{18}$$
$$\mathbf{y}_i = h(\mathbf{x}_i) + \mathbf{v}_i \text{ for } i = k-N,\ldots,k \tag{19}$$
$$l_i(\mathbf{x}_i) = 0 \text{ for } i = k-N,\ldots,k. \tag{20}$$

Here, $\mathbf{Q}$ is the process noise covariance and $\mathbf{R}$ is the measurement noise covariance. The estimate at the first time instance in the horizon is $\mathbf{x}_{k-N}^-$ with covariance $\mathbf{P}$, thus the third term in the cost function describes the arrival cost. The MHE minimizes a weighted sum of the noise over a moving time horizon which is shifted every time a new measurement is available as illustrated in Fig. 1. Substituting for (15) and (16) into (17) and adopting the notation $\mathbf{a}^\top\mathbf{B}\mathbf{a} = \|\mathbf{a}\|_{\mathbf{B}}^2$ gives the alternative formulation

$$\begin{aligned}\underset{\mathbf{x}_{k-N},\ldots,\mathbf{x}_k}{\text{minimize}} \; & \frac{1}{2}\sum_{i=k-N}^{k-1}\|\mathbf{x}_{i+1} - f(\mathbf{x}_i)\|_{\mathbf{Q}^{-1}}^2 \\ & + \frac{1}{2}\sum_{i=k-N}^{k}\|\mathbf{y}_i - h(\mathbf{x}_i)\|_{\mathbf{R}^{-1}}^2 \\ & + \frac{1}{2}\left\|\mathbf{x}_{k-N}^- - \mathbf{x}_{k-N}\right\|_{\mathbf{P}^{-1}}^2\end{aligned} \tag{21}$$

subject to

$$l_i(\mathbf{x}_i) = 0 \text{ for } i = k-N,\ldots,k. \tag{22}$$

We aim to estimate the pose of a body following random walk dynamics, meaning that the velocities of the body are modeled as a first-order Markov process. This dynamic system is formulated and applied for spacecraft pose estimation with dual quaternions using EKF in Filipe et al. (2015) and applied in Deng et al. (2016) to formulate an UKF with dual quaternions. Note that these dynamics can also be used to describe the motion of drones, aircraft, ground vehicles and marine vessels and may also have application in visual tracking and handheld camera mapping.

3.1 Velocity Measurement

Consider the discrete dynamic system in (13), a measurement $\tilde{\boldsymbol{\omega}}^B_{m,k}$ of the dual velocity of the body $\tilde{\boldsymbol{\omega}}^B_k$ is modeled as

$$\begin{aligned} \tilde{\boldsymbol{\omega}}^B_{m,k} &= \tilde{\boldsymbol{\omega}}^B_k + \tilde{\mathbf{b}}_{\omega,k} + \tilde{\mathbf{w}}_{\omega,k}, \quad [\tilde{\mathbf{w}}_{\omega,k}] \sim \mathcal{N}(0, \mathbf{Q}_\omega) \\ \tilde{\mathbf{b}}_{\omega,k+1} &= \tilde{\mathbf{b}}_{\omega,k} + h\tilde{\mathbf{w}}_{b,k}, \quad [\tilde{\mathbf{w}}_{b,k}] \sim \mathcal{N}(0, \mathbf{Q}_b), \end{aligned} \tag{23}$$

where $\tilde{\mathbf{w}}_{\omega,k}$ is the measurement noise and $\tilde{\mathbf{b}}_{\omega,k}$ is the dual bias driven by zero-mean Gaussian white noise $\tilde{\mathbf{w}}_{b,k}$. Note that the dual measurement vector $\tilde{\boldsymbol{\omega}}^B_{m,k} = \boldsymbol{\omega}^B_{m,k} + \varepsilon \mathbf{v}^B_{m,k}$ consist of an angular velocity measurement $\boldsymbol{\omega}^B_{m,k}$, that can come from a body-fixed gyroscope, and a linear velocity measurement $\mathbf{v}^B_{m,k}$ that can come from a vision- or GPS-system. Inserting for (13) into (23) and isolating the noise gives the cost

$$\mathbf{J}_\mathbf{Q} = \frac{1}{2}\sum_{i=k-N}^{k-1} \left\| \begin{matrix} \tilde{\boldsymbol{\omega}}_{m,i} - \frac{4}{h}\mathrm{cay}^{-1}\left(\tilde{\mathbf{q}}^*_i \otimes \tilde{\mathbf{q}}_{i+1}\right) - \tilde{\mathbf{b}}_{\omega,i} \\ \frac{1}{h}\left(\tilde{\mathbf{b}}_{\omega,i+1} - \tilde{\mathbf{b}}_{\omega,i}\right) \end{matrix} \right\|^2_{\mathbf{Q}^{-1}}, \tag{24}$$

where $\mathbf{Q} = \mathrm{diag}\left(\mathbf{Q}_\omega,\ \mathbf{Q}_b\right)$.

3.2 Pose Measurement

A pose measurement $\tilde{\mathbf{q}}_{m,k}$ of $\tilde{\mathbf{q}}_k$ can come from a vision based system or a system of combined sensors, including GPS and inertial measurement systems. For simplicity, we assume that the noise coming from the different sensors involved in the pose measurement can be modeled as Gaussian white-noise acting on the *roll-pitch-yaw* angles and *x-y-z* position parameters of the pose, which gives a physical interpretation of the noise. It is, however, not straightforward to model the relation of the measurement $\tilde{\mathbf{q}}_{m,k}$ and such noise due to the unit constraint of the dual quaternion. Enforcing the unit constraint may alter the distribution of the noise.

First, we consider the approach presented in Filipe et al. (2015), where Gaussian noise is added to the vector parts of the unit dual quaternion and then the scalar parts are recovered such that a unit dual quaternion is obtained. Recalling that

$$\tilde{\mathbf{q}}_{m,k} = \eta_{m,k} + \boldsymbol{\sigma}_{m,k} + \varepsilon\left(\eta'_{m,k} + \boldsymbol{\sigma}'_{m,k}\right), \tag{25}$$

the measurement relation using additive noise is

$$\begin{aligned} \boldsymbol{\sigma}_{m,k} + \varepsilon\boldsymbol{\sigma}'_{m,k} &= \left(\boldsymbol{\sigma}_k + \varepsilon\boldsymbol{\sigma}'_k\right) + \tilde{\mathbf{w}}_{q,k} \\ [\tilde{\mathbf{w}}_{q,k}] &\sim \mathcal{N}(0, \mathbf{R}). \end{aligned} \tag{26}$$

where $\tilde{\mathbf{w}}_{q,k}$ is a dual noise vector. The full unit dual quaternion $\tilde{\mathbf{q}}_{m,k}$ can be recovered through the relations

$$\tilde{\mathbf{q}} = \begin{cases} \sqrt{1 - \|\boldsymbol{\sigma}\|^2} + \boldsymbol{\sigma} \\ +\varepsilon\left(\dfrac{-\boldsymbol{\sigma}^\top\boldsymbol{\sigma}'}{\sqrt{1-\|\boldsymbol{\sigma}\|^2}} + \boldsymbol{\sigma}'\right), & \text{if } \|\boldsymbol{\sigma}\|^2 < 1 \\ \dfrac{1}{\sqrt{1+\|\boldsymbol{\sigma}\|^2}} + \dfrac{\boldsymbol{\sigma}}{\sqrt{1+\|\boldsymbol{\sigma}\|^2}} \\ +\varepsilon\left(\dfrac{-\boldsymbol{\sigma}^\top\boldsymbol{\sigma}'}{1/\sqrt{1+\|\boldsymbol{\sigma}\|^2}} + \boldsymbol{\sigma}'\right), & \text{if } \|\boldsymbol{\sigma}\|^2 \geq 1. \end{cases} \tag{27}$$

Fig. 2 shows histograms of 100000 simulations of (26) where the dual noise vector $[\tilde{\mathbf{w}}_{q,k}] \sim \mathcal{N}(0, 0.2\mathbf{I})$ is generated with the built-in MATLAB function *normrnd*. The full unit dual quaternion is recovered through (27), then the *x-y-z* positions and *roll-pitch-yaw* angles are extracted through (2) and plotted in the histograms. In Fig. 2a the true pose is $[\tilde{\mathbf{q}}] = [1\ 0\ 0\ 0\ 0\ 0\ 0\ 0]^\top$ and it can be seen that all parameters are normally distributed about the true value. In Fig. 2b the true pose is set to $[\tilde{\mathbf{q}}] = [0\ 0\ 0\ 1\ 0\ 0\ 0\ 0]^\top$ such that $\|\boldsymbol{\sigma}\|^2 = 1$, which corresponds to the *yaw* parameter being equal to π. Here it can be seen that the yaw parameter is not normally distributed about $\pm\pi$ and that the other parameters also are affected. This occurs due to the normalization when $\|\boldsymbol{\sigma}\|^2 \geq 1$ in (26). The normalization causes the distributions to become less Gaussian as $\|\boldsymbol{\sigma}\|^2$ approaches 1. These effects are minimized in Filipe et al. (2015) by ensuring that $\|\boldsymbol{\sigma}\|^2$ is close to 0 by formulating error dynamics.

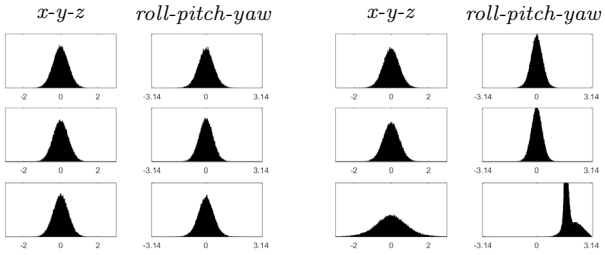

(a) $[\tilde{\mathbf{q}}] = [1\ 0\ 0\ 0\ 0\ 0\ 0\ 0]^\top$ (b) $[\tilde{\mathbf{q}}] = [0\ 0\ 0\ 1\ 0\ 0\ 0\ 0]^\top$

Fig. 2. Histograms showing position and attitude parameters after 100000 simulations of (26) for two cases of $\tilde{\mathbf{q}}$.

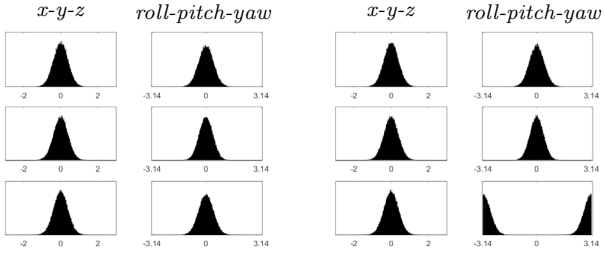

(a) $[\tilde{\mathbf{q}}] = [1\ 0\ 0\ 0\ 0\ 0\ 0\ 0]^\top$ (b) $[\tilde{\mathbf{q}}] = [0\ 0\ 0\ 1\ 0\ 0\ 0\ 0]^\top$

Fig. 3. Histograms showing position and attitude parameters after 100000 simulations of (28) for two cases of $\tilde{\mathbf{q}}$.

Next, we propose an approach where the dual noise vector $\tilde{\mathbf{w}}_{q,k}$ represents a twist, and the unit dual quaternion of the twist is found using the Cayley transform. The measurement relation can then be modeled with multiplicative noise as

$$\tilde{\mathbf{q}}_{m,k} = \tilde{\mathbf{q}}_k \otimes \mathrm{cay}\left(\frac{1}{2}\tilde{\mathbf{w}}_{q,k}\right). \tag{28}$$

The simulated noise vectors in Fig. 2 are applied to (28) and the same histograms are generated in Fig. 3. It can be seen in Fig. 3a that the parameters are normally distributed about the true value and produce similar results as in Fig. 2a. In Fig. 3b however, it can be seen that the *yaw* parameter is normally distributed about $\pm\pi$ and that the other parameters and not affected, even if $\|\boldsymbol{\sigma}\|^2 = 1$. This shows that this approach generates Gaussian measurements and are valid for all poses.

The cost of the pose measurements is found by isolating for the noise in (28)

$$\mathbf{J_R} = \frac{1}{2}\sum_{i=k-N}^{k} \left\| 2\text{cay}^{-1}\left(\tilde{\mathbf{q}}_i^* \otimes \tilde{\mathbf{q}}_{m,i}\right)\right\|^2_{\mathbf{R}^{-1}}. \tag{29}$$

3.3 Arrival Cost

The arrival cost describes the confidence of new data versus old data. It is obtained by time propagating the last state before the start of the window to the first state of the window and comparing the difference between propagated and observed data. The time propagated states are denoted $\tilde{\mathbf{q}}^-_{k-N}$ and $\tilde{\mathbf{b}}^-_{\omega,k-N}$ and obtained through the expectations of (13) and (23) as

$$\tilde{\mathbf{q}}^-_{k-N} = \mathbb{E}\left\{\tilde{\mathbf{q}}_{k-N}\right\} = \tilde{\mathbf{q}}_{k-N-1} \otimes \text{cay}\left(\frac{h}{4}\mathbb{E}\left\{\tilde{\boldsymbol{\omega}}^B_{k-N-1}\right\}\right), \tag{30}$$

where

$$\mathbb{E}\left\{\tilde{\boldsymbol{\omega}}^B_{k-N-1}\right\} = \tilde{\boldsymbol{\omega}}^B_{m,k-N-1} - \tilde{\mathbf{b}}_{\omega,k-N-1} \tag{31}$$

and

$$\tilde{\mathbf{b}}^-_{\omega,k-N} = \mathbb{E}\left\{\tilde{\mathbf{b}}_{\omega,k-N}\right\} = \tilde{\mathbf{b}}_{\omega,k-N-1}. \tag{32}$$

The difference between unit quaternions or unit dual quaternions can be obtained through simple subtraction as suggested in Vandersteen et al. (2013). However, this approach will violate the unit constraint and the subtraction will give no physical meaning. We consider the pose represented by $\tilde{\mathbf{q}}^-_{k-N}$ and $\tilde{\mathbf{q}}_{k-N}$, if they are similar then

$$\tilde{\mathbf{q}}^-_{k-N} \otimes \tilde{\mathbf{q}}^*_{k-N} = 1. \tag{33}$$

The arrival cost may then be formulated as

$$\mathbf{J_P} = \frac{1}{2}\left\| \begin{matrix} \tilde{\mathbf{q}}^-_{k-N} \otimes \tilde{\mathbf{q}}^*_{k-N} - 1 \\ \tilde{\mathbf{b}}^-_{\omega,k-N} - \tilde{\mathbf{b}}_{\omega,k-N} \end{matrix} \right\|^2_{\mathbf{P}^{-1}}, \tag{34}$$

where $\mathbf{P}$ describes the weight of the arrival cost. The bias state represent velocities and may be subtracted without loss of physical meaning.

We can now formulate the full MHE problem in terms of unit dual quaternions by combining the costs (24),(29) and (34) to the cost function $\mathbf{J}$ as

$$\mathbf{J} = \mathbf{J_Q} + \mathbf{J_R} + \mathbf{J_P} \tag{35}$$

and perform the constrained minimization

$$\underset{\substack{\tilde{\mathbf{q}}_{k-N},\ldots,\tilde{\mathbf{q}}_k \\ \tilde{\mathbf{b}}_{\omega,k-N},\ldots,\tilde{\mathbf{b}}_{\omega,k}}}{\text{minimize}} \quad \mathbf{J} \tag{36}$$

subject to

$$\tilde{\mathbf{q}}_i^* \otimes \tilde{\mathbf{q}}_i - 1 = 0, \text{ for } i = k-N,\ldots,k. \tag{37}$$

The constraints of the optimization ensures the algebraic constraint of the unit dual quaternion.

4. SIMULATION RESULTS

The proposed MHE was verified with simulated data and compared against the DQ-MEKF and the T-UKF. We considered the case where pose measurements were available as unit dual quaternions $\tilde{\mathbf{q}}_m$ and angular velocity measurements were available as vectors $\boldsymbol{\omega}^B_m$. The angular velocity measurements was represented as dual vectors $\tilde{\boldsymbol{\omega}}^B_m = \boldsymbol{\omega}^B_m + \varepsilon \mathbf{v}^B_m$ where the dual part representing linear velocity was set to zero, i.e $\tilde{\boldsymbol{\omega}}^B_m = \boldsymbol{\omega}^B_m$. This is the case for many inertial navigation applications where angular velocity may come from body fixed gyroscopes, while the linear velocity measurements may be unavailable.

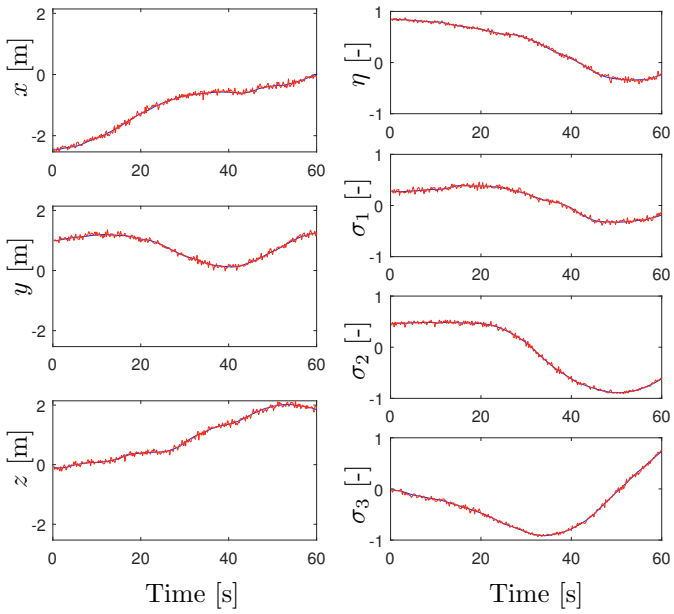

Fig. 4. Generated true pose (blue) and generated measurements (red). The dual values are converted to Euclidean position for physical interpretation.

The true velocities of the systems were generated according to the random walk process $\tilde{\boldsymbol{\omega}}^B_{k+1} = \tilde{\boldsymbol{\omega}}^B_k + \tilde{\mathbf{w}}_{t,k}$, where $[\tilde{\mathbf{w}}_{t,k}] \sim \mathcal{N}\left(0, 10^{-3}\mathbf{I}\right)$. The true pose, true bias, velocity measurements and pose measurements were then generated according to (13), (23) and (28) over a time interval of 60 s and a frequency of 5 Hz using the Gaussian number generator *normrnd* in Matlab. For the data generation, the process covariance $\mathbf{Q}_\omega$ was set to $\mathbf{Q}_\omega = \text{diag}(10^{-1}\mathbf{I}_{3\times3}, 10^{-9}\mathbf{I}_{3\times3})$, $\mathbf{Q}_b$ was set to $\mathbf{Q}_b = 10^{-3}\mathbf{I}_{6\times6}$ and the measurement covariance was set to $\mathbf{R} = 10^{-3}\mathbf{I}_{6\times6}$. The data generation was initialized with $[\tilde{\boldsymbol{\omega}}^B_0] \sim \mathcal{N}\left(0, 0.25\mathbf{I}\right)$, $\tilde{\mathbf{q}}_0 = \text{cay}\left(\frac{1}{2}\tilde{\mathbf{a}}\right)$, where $[\tilde{\mathbf{a}}] \sim \mathcal{N}\left(0, \mathbf{I}\right)$ and $\tilde{\mathbf{b}}_0 = [0\ 0\ 0\ 0\ 0\ 0]^\top$. An example sequence of the generated true pose and pose measurement with the given parameters is plotted in Fig. 4.

To make a fair comparison between the three estimators, the measurement relations suggested in the DQ-MEKF and the T-UKF were replaced with (28). The continuous process dynamics are similar for all three estimators and the discrete dynamics was implemented with (13) and (23). For the filtering, the process covariance of the bias state was increased to $\mathbf{Q}_b = \text{diag}(10^{-3}\mathbf{I}_{3\times3}, 10^{-1}\mathbf{I}_{3\times3})$ to compensate for the missing linear velocity measurements, this was also suggested in Filipe et al. (2015). The covariance tuning parameters $\mathbf{Q}_\omega$ and $\mathbf{R}$ were known from the data generation process. For generating sigma points in the T-UKF, the tuning parameter κ was set to $\kappa = 3 - n^a$ as suggested in Deng et al. (2016), where n^a is the dimension of the augmented state. The initial state estimates of the DQ-MEKF and the T-UKF were set equal to the true initial states from the data generation, $\hat{\tilde{\mathbf{q}}}_0 = \tilde{\mathbf{q}}_0$ and $\hat{\tilde{\mathbf{b}}}_0 = \tilde{\mathbf{b}}_0$. The initial state covariance were set to $\mathbf{P}_0 = 10^{-9}\mathbf{I}_{12\times12}$ for both the DQ-MEKF and the T-UKF.

The proposed MHE estimator was implemented in Matlab using the numeric optimization library CasADi (Andersson, 2013) and solved with the NLP method from CasADi. We allowed full convergence for each prob-

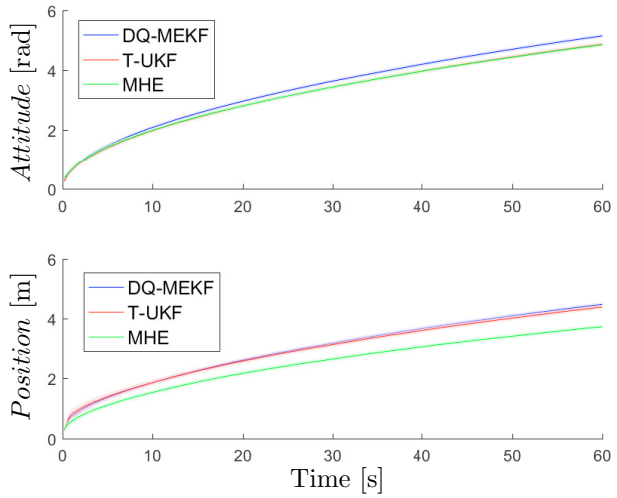

Fig. 5. RSS error for 100 simulations. The solid line is the mean of the error while the shaded area represent the standard deviation.

lem and the horizon included $N = 7$ pose measurements. The weighting matrix for the arrival cost was tuned through trial and error and was set to $\mathbf{P} = \text{diag}\left(\infty\mathbf{I}_{4\times4},\ 4\mathbf{I}_{4\times4}\ 5\times10^{-4}\mathbf{I}_{6\times6}\right)$

We compared the performance of the three estimators with 100 Monte Carlo simulations where a new data sequence were generated for each simulation. The error in attitude was computed as $2\arccos(\eta_\delta)$, where $\tilde{\mathbf{q}}_\delta = \hat{\tilde{\mathbf{q}}}_k^* \otimes \tilde{\mathbf{q}}_k = \eta_\delta + \boldsymbol{\sigma}_\delta + \varepsilon\,(\eta'_\delta + \boldsymbol{\sigma}'_\delta)$ and the error in position was computed as $\|\mathbf{r}_k - \hat{\mathbf{r}}_k\|$ where $\mathbf{r}_k = 2\mathbf{q}'_k \otimes \mathbf{q}_k^*$. The accumulated root sum squared (RSS) errors are plotted in Fig. 5, while the mean and standard deviation of the RSS error after 60 s are shown in table 1.

From Fig. 5 it can be seen that the DQ-MEKF and T-UKF produce similar results, which is consistent with the results presented in Deng et al. (2016). The MHE does not give any advantage in the attitude estimates when angular velocity measurements are available, however, it performs significantly better for the position estimation. Certainly, the performance of the MHE is affected by the tuning parameters N and $\mathbf{P}$, and the MHE may perform worse if these are neglected.

Table 1. RSS error for 100 simulations after 60s.

	DQ-MEKF		T-UKF		MHE	
	mean	s.d.	mean	s.d	mean	s.d.
Attitude [rad]	5.149	0.067	4.883	0.070	4.850	0.067
Position [m]	4.470	0.071	4.383	0.079	3.729	0.081

It is noted that the MHE have to solve an optimization problem every time a new measurement is available, which is computationally costly. Also, UKFs are in general more computationally costly than EKFs, due to the propagation of multiple sigma points. This indicates that the accuracy of the estimation comes at the expense of computation.

5. CONCLUSION

We have formulated a moving horizon estimator (MHE) for pose estimation with unit dual quaternions, where the suggested cost function is formulated in terms of the quaternion product so that the unit constraint of the dual quaternion is satisfied. In addition, we have suggested a measurement model where the noise represents a twist that is mapped to a unit dual quaternion using the Cayley transform. The proposed MHE was compared with the DQ-MEKF and the T-UKF through simulations and the MHE produced more accurate results for the position estimation.

Finally, it is noted that the MHE also estimates the angular and linear velocity of the system in the bias state, which may be required when implementing a control law.

REFERENCES

Andersson, J. (2013). *A General-Purpose Software Framework for Dynamic Optimization*. PhD thesis, Arenberg Doctoral School, KU Leuven, Department of Electrical Engineering (ESAT/SCD) and Optimization in Engineering Center, Kasteelpark Arenberg 10, 3001-Heverlee, Belgium.

Bayro-Corrochano, E. and Zhang, Y. (2000). The motor extended Kalman filter: A geometric approach for rigid motion estimation. *Journal of Mathematical Imaging and Vision*, 13(3), 205–228.

Chaturvedi, N.A., Sanyal, A.K., and McClamroch, N.H. (2011). Rigid-body attitude control. *IEEE Control Systems*, 31(3), 30–51.

Deng, Y., Wang, Z., and Liu, L. (2016). Unscented Kalman filter for spacecraft pose estimation using twistors. *Journal of Guidance, Control, and Dynamics*, 1844–1856.

Filipe, N., Kontitsis, M., and Tsiotras, P. (2015). Extended Kalman filter for spacecraft pose estimation using dual quaternions. *Journal of Guidance, Control, and Dynamics*, 38(9), 1625–1641.

Geebelen, K., Wagner, A., Gros, S., Swevers, J., and Diehl, M. (2013). Moving Horizon Estimation with a huber penalty function for robust pose estimation of tethered airplanes. In *American Control Conference (ACC), 2013*, 6169–6174. IEEE.

Goddard, J.S. (1997). *Pose and motion estimation from vision using dual quaternion-based extended Kalman filtering*. Ph.D. thesis, University of Tennessee, Knoxville.

Kristoffersen, T.T. and Holden, C. (2018). State and parameter estimation for a gas-liquid cylindrical cyclone. In *European Control Conference (ECC), 2018*. IEEE.

Lefferts, E.J., Markley, F.L., and Shuster, M.D. (1982). Kalman filtering for spacecraft attitude estimation. *Journal of Guidance, Control, and Dynamics*, 5(5), 417–429.

McCarthy, J.M. and Soh, G.S. (2010). *Geometric design of linkages*, volume 11. Springer Science & Business Media.

Polóni, T., Rohal-Ilkiv, B., and Johansen, T.A. (2015). Moving Horizon Estimation for Integrated Navigation Filtering. *IFAC-PapersOnLine*, 48(23), 519–526.

Rawlings, J. and Mayne, D. (2015). *Model Predictive Control: Theory and Design*. Nob Hill Pub.

Selig, J. (2010). Exponential and Cayley maps for dual quaternions. *Advances in applied Clifford algebras*, 20(3), 923–936.

Vandersteen, J., Diehl, M., Aerts, C., and Swevers, J. (2013). Spacecraft attitude estimation and sensor calibration using moving horizon estimation. *Journal of Guidance, Control, and Dynamics*.

Zu, Y., Lee, U., and Dai, R. (2014). Distributed motion estimation of space objects using dual quaternions. In *AIAA/AAS Astrodynamics Specialist Conference*, 2014-4296, 4–7.